Reactive Distillation in a Dividing Wall Column: Rate-Based Modeling and Simulation

ARTICLE *in* INDUSTRIAL & ENGINEERING CHEMISTRY RESEARCH · APRIL 2007

Impact Factor: 2.59 · DOI: 10.1021/ie0610344

Reactive Distillation in a Dividing Wall Column: Rate-Based Modeling and Simulation

Ivo Mueller and Eugeny Y. Kenig*

Department of Biochemical and Chemical Engineering, University of Dortmund, Emil-Figge-Str. 70, 44227 Dortmund, Germany

In this paper, a novel rate-based description of nonreactive and reactive dividing wall columns is presented. These highly integrated units promise advantages in the context of process intensification. Until now, published studies have been focused on the nonreactive columns, based on equilibrium stage models, whereas the modeling of both dividing wall columns and reactive dividing wall columns, using the rate-based approach, has not been done yet. In the presented model, special attention is given to phenomena that have not been considered in previous publications (e.g., heat transfer through the dividing wall). The model has been applied to a nonreactive, ternary alcohol mixture and successfully validated. The transesterification of carbonates has been identified as an interesting system for the reactive dividing wall column. This reaction system is equilibrium limited and characterized by high conversion, yet low selectivity. Initial simulation studies demonstrate that the selectivity can be significantly increased by means of the reactive dividing wall column. Besides, this highly integrated unit enables a more efficient separation of products and nonconverted reactants, resulting in a reduction in the separation unit number.

1. Introduction

Process intensification represents an important trend in chemical engineering and process technology attracting more and more attention of both industry and the research community. Among the benefits from the process intensification are reduction in equipment and plant size, improvements in process efficiency and safety, decreased waste and energy consumption and, consequently, better process economics.

One of the most promising ways for the process intensification is to deliberately integrate different phenomena or operations. In the past decades, the chemical process industries have shown a permanently increasing interest in the development of integrated processes combining reaction and separation mechanisms in one single unit (the so-called "reactive separations").[1] Reactive distillation represents probably the most important example of such integration. The advantages of reactive distillation include the following: (i) increased yield, because of overcoming chemical and thermodynamic equilibrium limitations; (ii) increased selectivity via suppression of undesired consecutive reactions; (iii) reduced energy consumption via direct heat integration, in the case of exothermic reactions; (iv) avoidance of hot spots by simultaneous liquid evaporation; and (v) ability to separate close boiling components.

Along with reactive separations, there are also other examples of process integration available, in which different separation units are linked together. For the separation of ternary mixtures, the well-known Petlyuk column configuration, which consists of two fully thermally coupled distillation columns, has been developed.[2] Compared to serial sequences of conventional columns, this column design offers better thermodynamic efficiency, reducing energy costs.[3] Condenser and reboiler of the first column (called the "prefractionator") are replaced by additional thermal links (vapor and liquid stream) with the second column (the "main column"), which additionally results in a capital cost decrease.

* To whom correspondence should be addressed. Tel.: +49 231/755-2357. Fax:+49 231/755-3035. E-mail: e.kenig@bci.uni-dortmund.de.

The Petlyuk configuration can also be realized in a single shell to yield the so-called "dividing wall column".[4] This is achieved when a vertical partition (wall) is introduced into a distillation column to arrange a prefractionator and a main column inside a single structure. The dividing wall columns have the following advantages:[5] (i) high purity for all three product streams reached in one single column; (ii) higher thermodynamic efficiency than that for serial column sequences, because of the reduced remixing effects, with respect to the middle component; and (iii) reduced number of equipment units.

The dividing wall columns have not been used extensively in industry yet, because of a lack of experience in design and control; however, their number has been growing constantly (40 units in 2004 worldwide).[6]

Both reactive distillation columns and dividing wall columns are further developments of a conventional distillation unit. On the other hand, they represent two different ways of integration. In this work, we address a new process integration idea, by combining reactive distillation and dividing wall column principles. The resulting integrated unit can be called the "reactive dividing wall column",[7,8] which combines both integration types (Figure 1).

2. Reactive Dividing Wall Column

The reactive dividing wall column features a very high degree of integration; however, this configuration must be thoroughly examined to ascertain whether it can lead to additional synergy effects. The configuration of dividing wall columns allows three high-purity product streams in a single column. Therefore, the following reactive systems can be considered relevant for this type of process integration:

(1) Reactive systems with more than two products (e.g., with consecutive and side reactions), which should be obtained as a pure fraction each;

(2) Reactive systems with nonreacting components and with desired separation of both products and inert components; and

(3) Reactive systems with an excess of a reagent, which should be separated with sufficient purity before being recycled.

10.1021/ie0610344 CCC: $37.00
Published on Web 04/28/2007

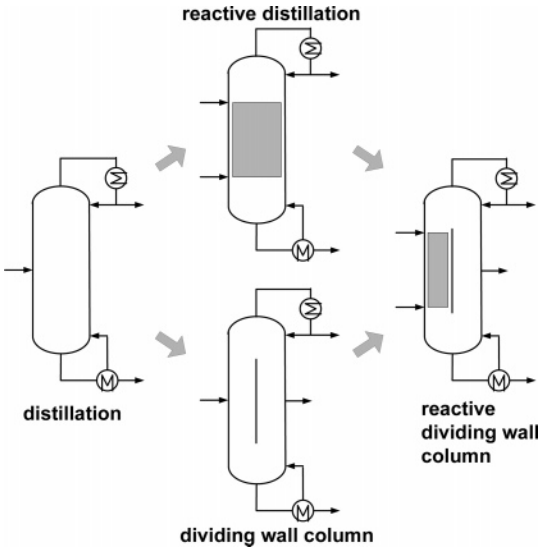

Figure 1. Schematic showing the path from a distillation column to a reactive dividing wall column (gray area represents the reactive zone).

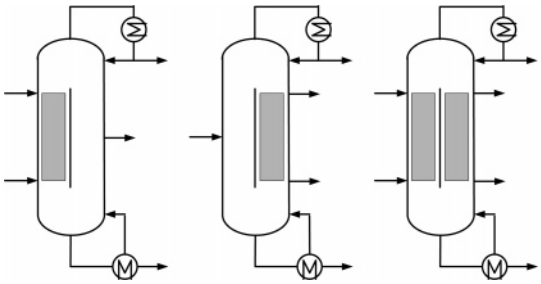

Figure 2. Examples of reactive zone arrangements (gray area).

Similar to the conventional reactive distillation, the process in a reactive dividing wall column can be catalyzed either homogeneously or heterogeneously. An advantage of the heterogeneous catalysis is the possibility to locate the reaction zone exactly. Additional possibilities to optimize the entire arrangement of reacting and separation zones inside the column are related to its subdivision by the dividing wall (Figure 2). By catalyst immobilization, product impurities are avoided and expensive recycling of the catalyst is not required. However, general disadvantages of heterogeneously catalyzed processes should be borne in mind, e.g., limited catalyst lifetime due to deactivation usually caused by undesired reaction products and increased operating temperature. At the moment, no industrial application of reactive dividing wall columns is known; however, this idea has been already approached in a few patents (see, e.g., Kaibel[9] and Hill et al.[10]).

3. Modeling

In previous publications, nonreactive dividing wall columns have been often described as a combination of single columns, which are linked together by vapor and liquid streams to imitate the dividing wall column.[11] The applied column models are mostly based on the equilibrium stage concept, which requires the following assumptions to be made: (i) the mass-transfer resistances of all components are equal (e.g., using the height equivalent to a theoretical plate (HETP) value), and (ii) no heat transfer occurs between the prefractionator and the main column through the dividing wall. Besides, vapor distribution below the dividing wall is often treated ideally (no pressure drop influence on vapor distribution close to the dividing wall).

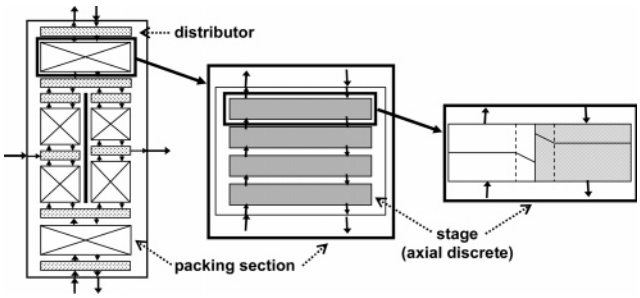

Figure 3. Column structure, discretized packing section, and a column stage (left, middle, and right panels, respectively), as described by the film model.

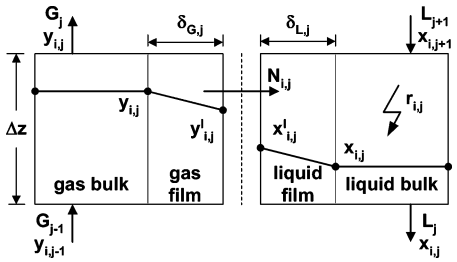

Figure 4. Film model for a reactive packing discrete (stage).

However, it was shown that the application of the equilibrium stage concept to complex systems is nontrivial, even in conventional distillation.[12] Thus, it is preferable to apply the so-called "rate-based stage model", taking account of the actual mass- and heat-transfer rates and process hydrodynamics.[13,14]

The model structure of the dividing wall column developed in this work uses the description of the column internals arrangement, which is very close to reality. The internals are composed of packing sections and distributors between them (Figure 3). In the distributor model, mass and heat transport between the liquid and vapor phases is not considered. However, the distributors are used to connect the feed and side streams with the column. Besides, the distributors have another function: namely, to split and mix the streams at the upper and lower end of the dividing wall. For modeling purposes, each packing section is discretized onto smaller segments (stages). Each single stage is described via the film model first suggested by Lewis and Whitman[15] (see Figure 3) (the model has since been well-established). In a similar way, one can consider a dividing wall column equipped with trays, whereas each tray is related to one rate-based stage.

In addition to the phenomena occurring in the nonreactive dividing wall column, the reactive dividing wall column includes liquid-phase reactions that occur in the reactive zone. Therefore, in the following section, we present a general rate-based stage model, describing both nonreactive and reactive cases.

3.1. Main Mass-Transfer Equations. A detailed model for heterogeneously catalyzed reactive distillation processes has been suggested by Górak and Hoffmann[16] and further developed to cover different reactive and nonreactive separation processes and various column configurations.[17]

The applied rate-based stage concept is illustrated in Figure 4. The heterogeneously catalyzed reactions in the liquid bulk phase are treated as pseudo-homogeneous ones. For the steady-state operation, the component balances for the vapor and liquid phase at a stage j are written as

$$0 = G_{j-1}y_{i,j-1} - G_j y_{i,j} - N_{i,j}a_j A_j \Delta z_j \quad (1)$$

$$0 = L_{j+1}y_{i,j+1} - L_j x_{i,j} + (N_{i,j}a_j + r_{i,j}\Psi_{cat}\rho_{cat})A_j \Delta z_j \quad (2)$$

In eqs 1 and 2, it is assumed that mass transfer from the vapor phase to the liquid phase is positive. Generally, eq 2 describes both reactive and nonreactive cases. For the stages outside the reaction zone (no reaction), the reaction term $r_{i,j}$ is set equal to zero. The molar fluxes $N_{i,j}$ are related to the diffusional fluxes by

$$J^{\mathrm{L}}_{i,j} + x_{i,j}\sum_{k=1}^{n} N_{k,j} = N_{i,j} = J^{\mathrm{G}}_{i,j} + y_{i,j}\sum_{k=1}^{n} N_{k,j} \quad (\text{for } i = 1\,, ..., n-1) \quad (3)$$

and the following summation conditions are valid:

$$\sum_{i=1}^{n} x_{i,j} = \sum_{i=1}^{n} y_{i,j} = 1 \quad (4)$$

In this work, two different approaches for the mass-transfer rates are used: namely, a rigorous description using the Maxwell−Stefan equations and an approach using Fick's law with effective diffusivities.

For the Maxwell−Stefan approach, the method of Krishna and Standard[18] is used to relate the multicomponent mass-transfer rates to binary mass-transfer coefficients. The diffusional fluxes can be calculated from

$$(J^{\mathrm{L}})_j = -c^{\mathrm{L,av}}_{t,j}[k^{\mathrm{av}}_{\mathrm{L}}]_j[\Gamma]_j(x - x^{\mathrm{I}})_j \quad (5)$$

$$(J^{\mathrm{G}})_j = -c^{\mathrm{G,av}}_{t,j}[k^{\mathrm{av}}_{\mathrm{G}}]_j(y^{\mathrm{I}} - y)_j \quad (6)$$

where the matrix of the mass-transfer coefficients is defined as

$$[k^{\mathrm{av}}]_j = [R^{\mathrm{av}}]_j^{-1} \quad (7)$$

with

$$R^{\mathrm{L,av}}_{i,i,j} = \frac{x^{\mathrm{av}}_{i,j}}{\kappa^{\mathrm{L}}_{i,n,j}} + \sum_{\substack{k=1\\k\neq i}}^{n}\frac{x^{\mathrm{av}}_{k,j}}{\kappa^{\mathrm{L}}_{i,k,j}} \quad (i = 1, ..., n-1) \quad (8)$$

$$R^{\mathrm{L,av}}_{i,k,j} = -x^{\mathrm{av}}_{i,j}\left(\frac{1}{\kappa^{\mathrm{L}}_{i,k,j}} - \frac{1}{\kappa^{\mathrm{L}}_{i,n,j}}\right) \quad (i, k = 1, ..., n-1\ (i \neq k)) \quad (9)$$

$$R^{\mathrm{G,av}}_{i,i,j} = \frac{y^{\mathrm{av}}_{i,j}}{\kappa^{\mathrm{G}}_{i,n,j}} + \sum_{\substack{k=1\\k\neq i}}^{n}\frac{y^{\mathrm{av}}_{k,j}}{\kappa^{\mathrm{G}}_{i,k,j}} \quad (i = 1, ..., n-1) \quad (10)$$

$$R^{\mathrm{G,av}}_{i,k,j} = -y^{\mathrm{av}}_{i,j}\left(\frac{1}{\kappa^{\mathrm{G}}_{i,k,j}} - \frac{1}{\kappa^{\mathrm{G}}_{i,n,j}}\right) \quad (i, k = 1, ..., n-1\ (i \neq k)) \quad (11)$$

The binary mass-transfer coefficients ($\kappa_{i,k}$) can be extracted from suitable mass-transfer correlations, using the appropriate Maxwell−Stefan diffusion coefficients ($Đ_{i,k}$).[18] According to the linearized theory,[19,20] the matrices are evaluated using average mole fractions, defined as

$$x^{\mathrm{av}}_{i,j} = \frac{x_{i,j} + x^{\mathrm{I}}_{i,j}}{2} \quad (i = 1, ..., n) \quad (12)$$

$$y^{\mathrm{av}}_{i,j} = \frac{y^{\mathrm{I}}_{i,j} + y_{i,j}}{2} \quad (i = 1, ..., n) \quad (13)$$

Similarly, the physical properties of the films (e.g., average molar density, c_t^{av}) are calculated using these average compositions.

In the second approach, the diffusional fluxes are based on Fick's law:

$$(J^{\mathrm{L}})_j = -c^{\mathrm{L,av}}_{t,j}(k^{\mathrm{eff}}_{L})_j(x - x^{\mathrm{I}})_j \quad (14)$$

$$(J^{\mathrm{G}})_j = -c^{\mathrm{G,av}}_{t,j}(k^{\mathrm{eff}}_{\mathrm{G}})_j(y^{\mathrm{I}} - y)_j \quad (15)$$

In this case, the required effective mass-transfer coefficients are calculated from empirical correlations by implementing effective diffusivities D_i^{eff}; the latter can be derived from different methods (e.g., the method of Wilke−Chang).[21] Compared to the matrix-based calculation in the Maxwell−Stefan approach, the application of Fick's law provides a simpler equation system for the mass transfer, thus enhancing both convergence and simulation speed.

Phase equilibrium is assumed at the interface:

$$y^{\mathrm{I}}_{i,j} = K^{\mathrm{eq}}_{i,j}\, x^{\mathrm{I}}_{i,j} \qquad (i = 1, ..., n) \quad (16)$$

where vapor−liquid equilibrium constants $K^{\mathrm{eq}}_{i,j}$ are determined using particular thermodynamic models, e.g., UNIQUAC together with the extended Antoine equation for the vapor pressure.[21] The influence of the process hydrodynamics is directly taken into account by correlations for mass-transfer coefficients, specific contact area, liquid holdup and pressure drop (see, e.g., Bravo et al.[22,23]).

3.2. Main Heat-Transfer Equations. In the previous section, the mass balances of the rate-based stage model are given. Here, we address the phenomenon of the heat transfer in the column, including both the transfer within the stage and the heat conduction through the dividing wall, which represents a peculiar feature of this column configuration. The heat transfer through the wall can be a significant factor that influences the separation efficiency.[24]

In reality, the dividing wall is covered by a liquid−vapor mixture and, generally, it is difficult to make an exact estimation of a near-wall phase state. Therefore, in our model, we assume that the wall is covered by one phase only and consider two different cases. The first case is when the dividing wall is covered by the vapor phase from both sides, the second case is when both sides are covered with liquid. To model the heat-transfer phenomena, we must consider a complete cross section of the dividing wall column, because the left-side (prefractionator) and right-side (main column) stages are linked by the heat-transfer flux between them (Figure 5).

The energy balances for the entire cross-section can be subdivided onto the balances for the vapor and liquid phases, which are formulated as follows:

$$0 = G_{j-1}H_{\mathrm{G},j-1} - G_jH_{\mathrm{G},j} - q_j^{\mathrm{I}}a_jA_{\mathrm{col}}\Delta z \pm Q^{W}_{\mathrm{G},j} \quad (17)$$

$$0 = L_{j+1}H_{\mathrm{L},j+1} - L_jH_{\mathrm{L},j} + q_j^{\mathrm{I}}a_jA_{\mathrm{col}}\Delta z \pm Q^{W}_{\mathrm{L},j} \quad (18)$$

These equations are written for both the prefractionator and the main column. For the prefractionator, the last term in eqs 17 and 18 is negative, whereas for the main column, it is positive (cf. Figure 5). Similar to the mass transfer, the heat transfer from the vapor to the liquid phase is assumed positive. The heat flux across the vapor−liquid interface consists of a convective component and a conductive

component:

$$q_j^{\mathrm{I}} = \frac{\lambda_{\mathrm{G},j}}{\delta_{\mathrm{G},j}^{\mathrm{av}}}(T_{\mathrm{G},j} - T_j^{\mathrm{I}}) + \sum_{i=1}^{n} N_{i,j} H_{\mathrm{G},i,j} = \frac{\lambda_{\mathrm{L},j}}{\delta_{\mathrm{L},j}^{\mathrm{av}}}(T_j^{\mathrm{I}} - T_{\mathrm{L},j}) + \sum_{i=1}^{n} N_{i,j} H_{\mathrm{L},i,j} \quad (19)$$

The average film thickness (δ^{av}) for both the liquid and vapor film is needed to calculate the conductive interfacial heat transfer and can be derived as the weighted effective film thickness:

$$\delta_{\mathrm{L},j}^{\mathrm{av}} = \sum_{i=1}^{n} x_{i,j}\delta_{\mathrm{L},i,j} = \sum_{i=1}^{n} x_{i,j}\frac{D_{\mathrm{L},i,j}^{\mathrm{eff}}}{k_{\mathrm{L},i,j}^{\mathrm{eff}}} \quad (20)$$

$$\delta_{\mathrm{G},j}^{\mathrm{av}} = \sum_{i=1}^{n} y_{i,j}\delta_{\mathrm{G},i,j} = \sum_{i=1}^{n} y_{i,j}\frac{D_{\mathrm{G},i,j}^{\mathrm{eff}}}{k_{\mathrm{G},i,j}^{\mathrm{eff}}} \quad (21)$$

The heat flow rate across the dividing wall (Q_j^{W}) is dependent on the phases that are adjacent to this wall. For the liquid phase,

$$Q_{\mathrm{L},j}^{\mathrm{W}} = k_j^{\mathrm{W}}\Delta A^{\mathrm{W}}(T_{\mathrm{L},j}^{\mathrm{PF}} - T_{\mathrm{L},j}^{\mathrm{MC}}) \quad (22)$$

whereas for the vapor phase,

$$Q_{\mathrm{G},j}^{\mathrm{W}} = k_j^{\mathrm{W}}\Delta A^{\mathrm{W}}(T_{\mathrm{G},j}^{\mathrm{PF}} - T_{\mathrm{G},j}^{\mathrm{MC}}) \quad (23)$$

For a plane wall, the overall heat-transfer coefficient (k_j^{W}) for stage j can be calculated using the heat-transfer coefficients of the adjacent phases and the wall heat conduction coefficient:

$$\frac{1}{k_j^{\mathrm{W}}} = \frac{1}{\alpha_j^{\mathrm{W,PF}}} + \frac{s^{\mathrm{W}}}{\lambda_j^{\mathrm{W}}} + \frac{1}{\alpha_j^{\mathrm{W,MC}}} \quad (24)$$

The value of λ^{W} is dependent on the wall material and can be found in the literature. The estimation of heat-transfer coefficients α^{W}, however, is problematic, because no correlations for walls of distillation columns are available. On the other hand, neglecting the near-wall heat resistances may result in unrealistically large values of heat fluxes. As the first approximation, one can apply constant values of the overall heat-transfer coefficients.

3.3. Liquid and Vapor Split. The prefractionator and the main column exchange vapor and liquid streams above and below the dividing wall. Above the dividing wall (aDW), the ascending vapor streams from the prefractionator and main column are mixed, while the liquid stream from the main column is split into two streams, which further flow along both sides of the dividing wall. Below the dividing wall (bDW), these phenomena are contrary: the liquid streams are mixed and the vapor streams are split (Figure 6).

The mixing of both downstreaming liquid flows L^{bMC} (the main column side) and L^{bPF} (the prefractionator side) below the dividing wall to stream L^{bDW} is described as

$$L^{\mathrm{bDW}}x_i^{\mathrm{bDW}} = L^{\mathrm{bMC}}x_i^{\mathrm{bMC}} + L^{\mathrm{bPF}}x_i^{\mathrm{bPF}} \qquad (\text{for } i = 1, ..., n) \quad (25)$$

The mixed vapor stream G^{aDW} above the dividing wall (aDW) is calculated by

$$G^{\mathrm{aDW}}y_i^{\mathrm{aDW}} = G^{\mathrm{aMC}}y_i^{\mathrm{aMC}} + G^{\mathrm{aPF}}y_i^{\mathrm{aPF}} \qquad (\text{for } i = 1, ..., n) \quad (26)$$

whereas the following summation conditions are valid:

$$\sum_{i=1}^{n} x_i^{\mathrm{bDW}} = \sum_{i=1}^{n} y_i^{\mathrm{aDW}} = 1 \quad (27)$$

The temperatures of the liquid and vapor mixtures are calculated by means of enthalpy balances:

$$L^{\mathrm{bDW}}H_{\mathrm{L}}^{\mathrm{bDW}} = L^{\mathrm{bMC}}H_{\mathrm{L}}^{\mathrm{bMC}} + L^{\mathrm{bPF}}H_{\mathrm{L}}^{\mathrm{bPF}} \quad (28)$$

$$G^{\mathrm{bDW}}H_{\mathrm{G}}^{\mathrm{bDW}} = G^{\mathrm{aMC}}H_{\mathrm{G}}^{\mathrm{aMC}} + G^{\mathrm{aPF}}H_{\mathrm{G}}^{\mathrm{aPF}} \quad (29)$$

To describe the splitting, the so-called "split ratios" are defined as the ratio of the stream flow rate entering the prefractionator and the total stream flow rate:

$$\varphi_{\mathrm{L}} = \frac{L^{\mathrm{aPF}}}{L^{\mathrm{aDW}}} \quad (30)$$

$$\varphi_{\mathrm{G}} = \frac{G^{\mathrm{bPF}}}{G^{\mathrm{bDW}}} \quad (31)$$

In addition, the balances of the flow rates are required:

$$L^{\mathrm{aDW}} = L^{\mathrm{aMC}} + L^{\mathrm{aPF}} \quad (32)$$

$$G^{\mathrm{bDW}} = G^{\mathrm{bMC}} + G^{\mathrm{bPF}} \quad (33)$$

Both concentrations and temperatures remain unchanged for the split streams:

$$x_i^{\mathrm{aDW}} = x_i^{\mathrm{aMC}} = x_i^{\mathrm{aPF}} \qquad (\text{for } i = 1, ..., n) \quad (34)$$

$$y_i^{\mathrm{bDW}} = y_i^{\mathrm{bMC}} = y_i^{\mathrm{bPF}} \qquad (\text{for } i = 1, ..., n) \quad (35)$$

$$T_{\mathrm{L}}^{\mathrm{aDW}} = T_{\mathrm{L}}^{\mathrm{aMC}} = T_{\mathrm{L}}^{\mathrm{aPF}} \quad (36)$$

$$T_{\mathrm{G}}^{\mathrm{bDW}} = T_{\mathrm{G}}^{\mathrm{bMC}} = T_{\mathrm{G}}^{\mathrm{aPF}} \quad (37)$$

The liquid split ratio (φ_{L}) can be used as an adjustable control parameter for the dividing wall column. However, the vapor distribution cannot be easily controlled; rather, it represents a self-adjusting parameter, because the vapor distribution in a reactive dividing wall column must provide an equal pressure drop at both sides of the dividing wall:

$$\Delta p^{\mathrm{MC}} = \Delta p^{\mathrm{PF}} \quad (38)$$

In previous publications about the modeling of dividing wall columns, this issue was neglected. If pressure drop correlations are missing or for initialization purposes, the vapor split can be set equal to the cross-sectional area ratio, which is defined as

$$\phi_{\mathrm{Area}} = \frac{A^{\mathrm{PF}}}{A_t} \quad (39)$$

In reality, different liquid loads and gas capacities and, if applicable, different internals in the prefractionator and in the main column can cause very different vapor resistances at different sides of the wall. In this case, the real vapor split ratio

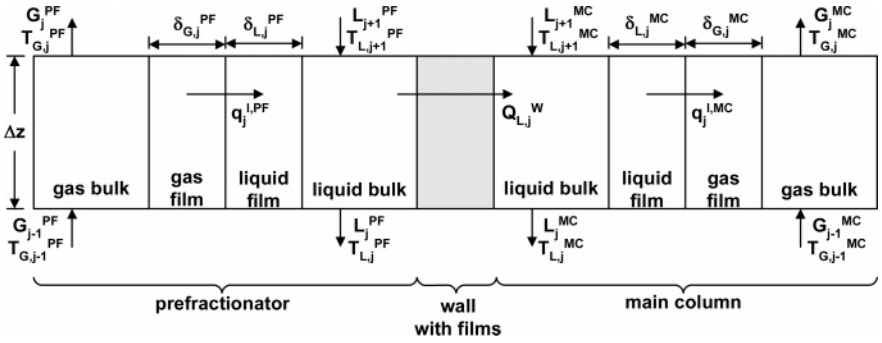

Figure 5. Heat transfer in a cross section of the dividing wall column for the case of the liquid−liquid heat transfer at the wall.

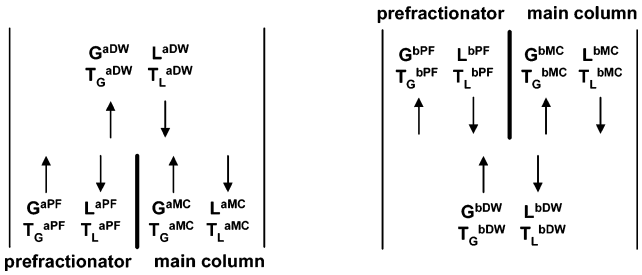

Figure 6. Liquid and vapor split above (left) and below (right) the dividing wall.

deviates from the cross-sectional area ratio, which influences the column performance.

4. Model Implementation

Discretization of the dividing wall column in the axial direction, in combination with the detailed rate-based approach, results in a large and highly nonlinear algebraic system of equations. Therefore, proper implementation and solution of the model equations is important.

The rate-based model described above is implemented into the ASPEN Custom Modeler (ACM) simulation environment. The ACM is an equation-oriented simulator that simultaneously solves the equation system for the entire flowsheet. For the considered complex problem, the availability of good starting values is usually a deciding factor. To generate the starting values, a simpler model has been used. The latter represents an extended equilibrium stage model, in which chemical reaction rates are taken into account simultaneously with the thermodynamic equilibrium assumption for the leaving streams.

5. Nonreactive Case

The developed model has been first applied to a nonreactive dividing wall column that was investigated by Abdul Mutalib et al.[25]

5.1. System. In the work by Abdul Mutalib et al.,[25] a ternary mixture methanol−isopropanol−butanol is analyzed. This mixture is relatively simple and has no miscibility gaps and no azeotropes. Therefore, we consider it to be an appropriate system for studying dividing wall arrangements. The boiling points of the pure components at atmospheric pressure are 64 °C (methanol), 82 °C (isopropanol), and 117 °C (butanol).

5.2. Column Setup. The pilot dividing wall column has a diameter of 0.305 m and an overall height of 10.97 m. The column is equipped with the structured Gempak 4A packing. The packing height in the main column is ∼8.7 m, and in the prefractionator, it is ∼3.8 m (Figure 7). With a number of theoretical stages per meter (NTSM) value of ∼3.7 m^{-1}, the

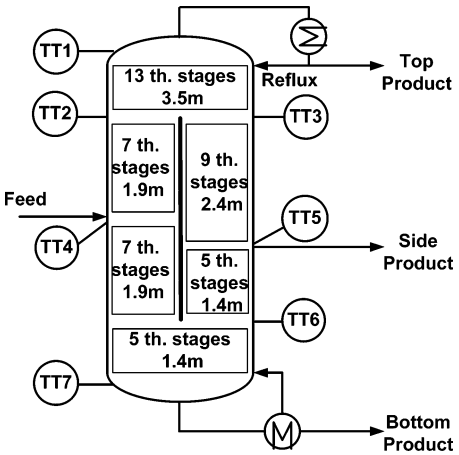

Figure 7. Experimental column setup (adapted from Abdul Mutalib et al.[25]).

Table 1. Data Set for Run 1

parameter	value
V_{Feed}	0.082 m^3/h
$x_{Methanol}$	0.342 mol/mol
$x_{Isopropanol}$	0.312 mol/mol
$x_{Butanol}$	0.346 mol/mol
T_{Feed}	78.5 °C
$V_{Top\ Reflux}$	0.156 m^3/h
$T_{Top\ Reflux}$	34.7 °C
$V_{Top\ Product}$	0.016 m^3/h
$V_{Side\ Product}$	0.029 m^3/h

total packing height in both parts of the column is thus equivalent to 47 theoretical stages, including the reboiler (cf. Figure 7). The dividing wall is slightly shifted to the feed side, which results in a larger cross-sectional area of the main column. The cross-sectional area ratio of the prefractionator to the total column is equal to 0.44. Liquid from the top section is split into two streams, flowing along the dividing wall, at a ratio of 4.8 (main column to prefractionator). The feed temperature is maintained at ∼78.5 °C by a temperature controller at the feed preheater. The top reflux is sub-cooled to ∼35 °C for safety reasons and to avoid methanol loss in the condenser venting line. The column works at atmospheric pressure. Liquid samples from the feed and the product streams are taken and analyzed off-line, using a gas chromatograph. The temperatures between the single packing segments are measured with resistance thermometers; the measurement points are indicated by the symbol "TT" in Figure 7.

5.3. Operating Conditions. The column feed in all experiments is close to the equimolar composition and is heated just below the mixture boiling point. As an example, the data on one selected experiment (denoted as "Run One" in the work of Abdul Mutalib et al.[25]) are given in Table 1.

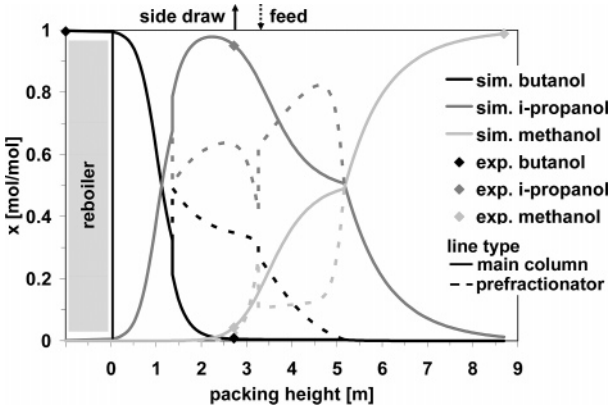

Figure 8. Simulated liquid-phase composition profiles and experimental data for Run 1.[25]

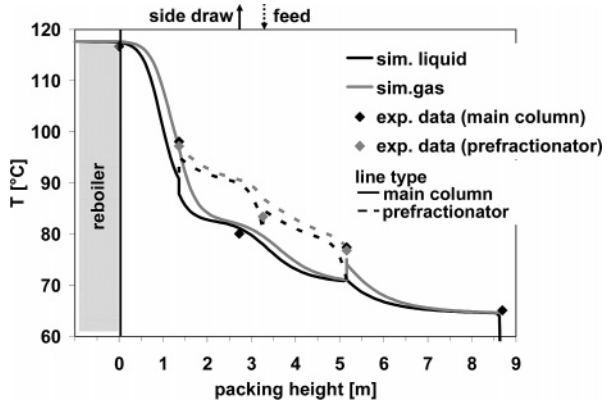

Figure 9. Simulated temperature profiles and experimental data for Run 1.[25]

5.4. Results. The simulations have been performed without any adjusting parameters. The heat transfer through the dividing wall for this specific validation case is not considered, because no accurate data for the heat-transfer coefficients are available. The pressure drop, liquid holdup, interfacial area, and mass-transfer coefficients for the Gempak 4A packing that has been used are calculated with the correlations of Rocha et al.[26,27] The thermodynamic properties are described by the UNIQUAC model.

5.4.1. Model Validation. In Figures 8 and 9, the calculated column profiles are compared with the pilot plant data taken from the work of Abdul Mutalib et al.[25] The pre-separation of the high-boiling component (butanol) and the low-boiling component (methanol) in the prefractionator can be seen in Figure 8. This facilitates the further separation in the main column, because it is almost reduced to the separation of two binary mixtures, namely, butanol−isopropanol in the lower part and methanol−isopropanol in the upper part of the main column. The splitting of the vapor flow below the dividing wall is almost identical to the cross-sectional area ratio, because the same packing type with low liquid loads is used at both sides of the dividing wall. In this case, the assumption of equal area ratios and vapor flow rate ratios is appropriate. The choice of the mass-transfer description approach—namely, Maxwell−Stefan or effective mass-transfer coefficients (cf. section 3.1)—has only a marginal influence on the simulation results.

A good agreement can be observed between the simulated and experimental data for the liquid-phase concentrations (Figure 8) and temperature (Figure 9). The maximum deviation between the simulated and measured product purities is <0.003 mol/mol, which is a good result. The average relative deviation between the experimentally measured and simulated temperatures is ∼1.9%, which is also a good value. The validation has also been successful for two other data sets taken from the work of Abdul Mutalib et al.[25] However, an additional verification of the model is necessary, in regard to different setups and operation conditions.

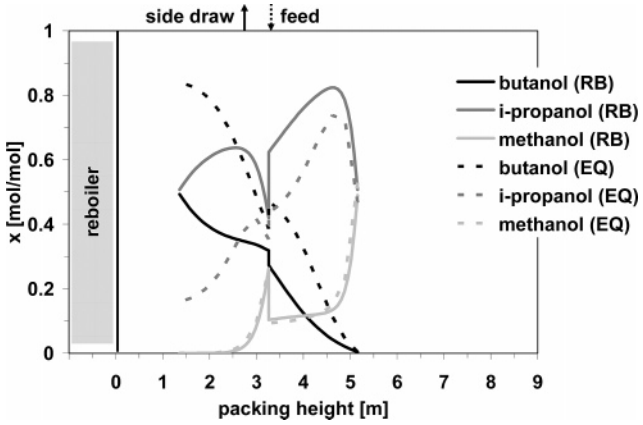

Figure 10. Modeling depth influence on the liquid-phase composition in the prefractionator.

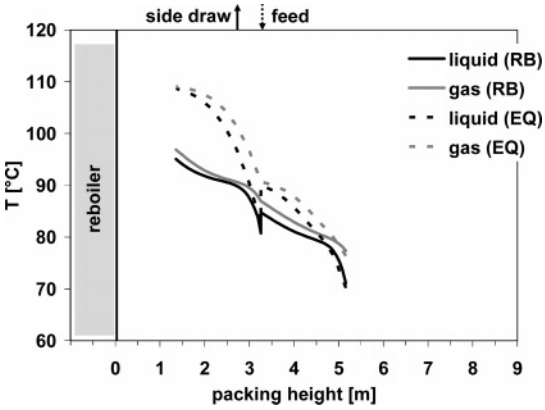

Figure 11. Modeling depth influence on the temperature in the prefractionator.

5.4.2. Rate-Based versus Equilibrium Stage Models. The comparison of the more rigorous rate-based stage (RB) model with the simplified equilibrium stage (EQ) model is often requested to decide on the necessary modeling depth. For this investigation, the required number of equilibrium (theoretical) stages is chosen according to the work of Abdul Mutalib et al.[25]

The simulation results for both approaches are shown in Figures 10−13. The difference in the concentration profiles within the prefractionator (Figure 10) is quite significant and, thus, the simulated temperature profiles also differ (Figure 11). Smaller deviations are observed in the main column (Figures 12 and 13).

It can be seen that the equilibrium stage model yields higher values of temperature and butanol concentration in the lower part of both the prefractionator and the main column. One may guess some overestimation of the separation efficiency of the column by the equilibrium stage model. This guess is supported by the work of Abdul Mutalib et al.[25] by a comparison of simulation results of the equilibrium stage model with experimental data. The liquid load (<7 $m^3\ m^{-2}\ h^{-1}$) and F-factor (<0.7 $Pa^{0.5}$) were quite low in these experiments; this could negatively influence the packing separation efficiency and, thus, reduce the relevant equilibrium stage number. Other reasons suggested by Abdul Mutalib et al.[25] are the small column diameter or the noncircular cross section of the packing beside the dividing wall.

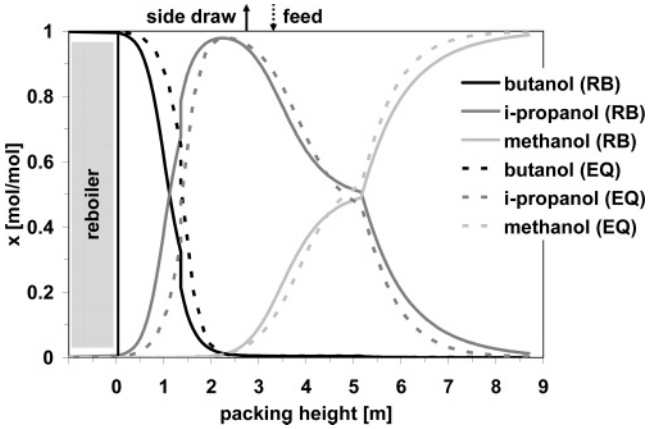

Figure 12. Modeling depth influence on the liquid-phase composition in the main column.

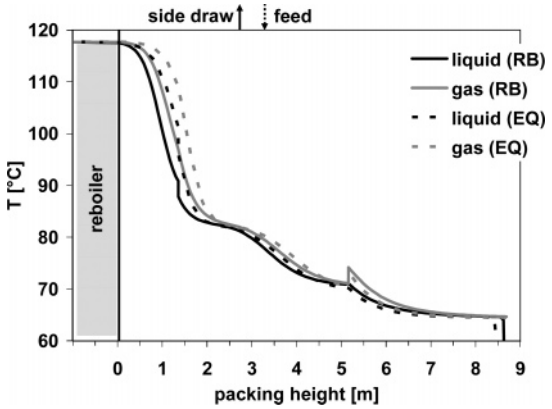

Figure 13. Modeling depth influence on the temperature in the main column.

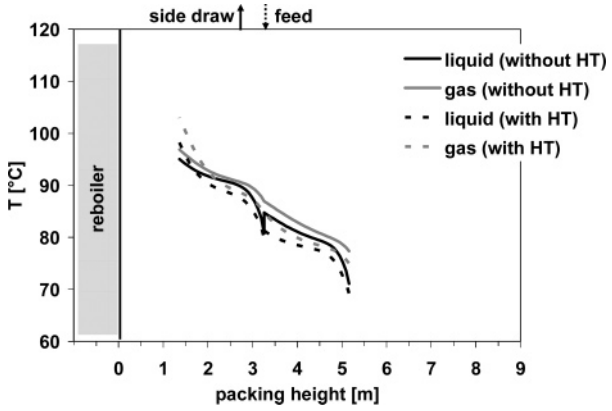

Figure 14. Influence of heat transfer through the dividing wall on the temperature in the prefractionator.

A final explanation is difficult, because of insufficient measurement data on the Gempak 4A packing.

5.4.3. Heat Transfer through the Dividing Wall. As the next step, the heat transfer through the wall has been analyzed. Although the additional thermal coupling of the prefractionator and the main column leads to a more-complex system of equations, no serious problems in reaching convergence have been encountered.

We have investigated and compared two different cases, namely, a column with an ideally isolated dividing wall (without heat transfer), which is thermodynamically equivalent to the Petlyuk configuration, and a column with a heat transfer through the wall estimated by the overall heat-transfer coefficient: $k^W = 600$ W/m^2 (with heat transfer). The composition profiles for

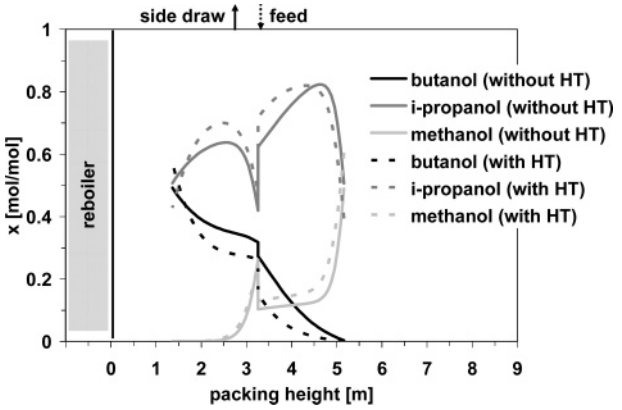

Figure 15. Influence of heat transfer through the dividing wall on the liquid-phase composition in the prefractionator.

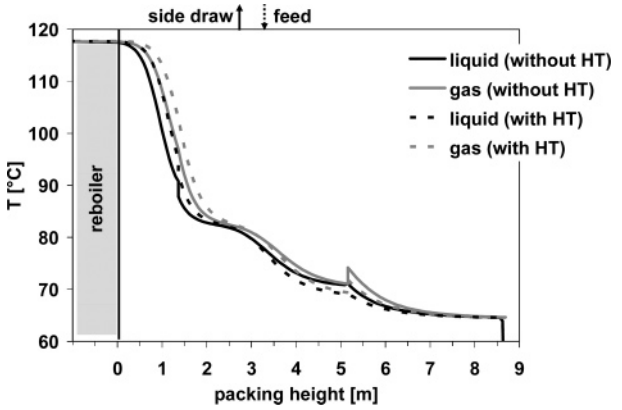

Figure 16. Influence of heat transfer through the dividing wall on the temperature in the main column.

the liquid phase and the temperature profiles are shown separately for the main column and the prefractionator in Figures 14−17, correspondingly.

The heat is transferred from the prefractionator to the main column. Significant deviations between the two cases can be easily recognized in the region of the prefractionator (Figures 14 and 15). In the upper and lower parts of the column, the deviations disappear (Figures 16 and 17). For this reason, the changes in the product streams are marginal (Figures 16). It is difficult to evaluate the role of the heat transfer with only few experimental results available. Thus, for a more solid conclusion, additional experimental data for the composition profiles inside the column are required.

6. Reactive Case

No data on the application of a reactive dividing wall column are available; therefore, the investigation had to be started from the beginning, with due account of the results obtained for the nonreactive case. It should be kept in mind that reactive systems are usually described by a very complex and highly nonlinear system of equations. Also, the calculation of the physicochemical data is more difficult, and, generally, the model becomes highly parameter-sensitive. Thus, the simulation of a reactive dividing wall column represents a demanding task. In this section, the simulation results are presented for a selected model column setup.

6.1. System. As a test system for the investigation of the reactive dividing wall column, the transesterification of dimethyl carbonate (DMC) with ethanol (EtOH) to diethyl carbonate (DEC) and methanol (MeOH) was found to be interesting.[8] DMC and DEC are important reactants and solvents for many

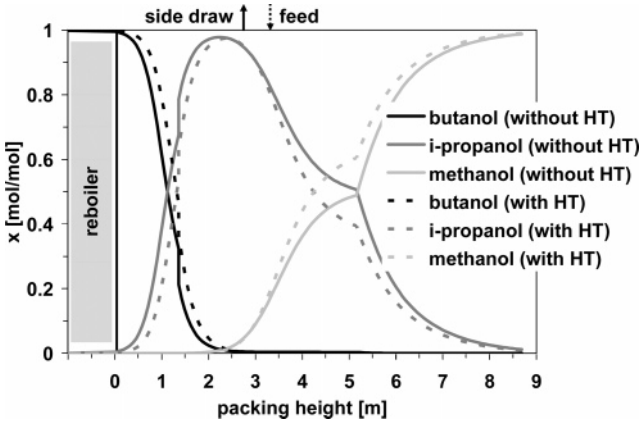

Figure 17. Influence of heat transfer through the dividing wall on the liquid-phase composition in the main column.

Table 2. Kinetic Parameters of eqs 42−45[a]

reaction	activation energy, E_A (J/mol)	frequency factor, k_0 (mol s^{-1} kg_{cat}^{-1})	equilibrium constant, K_{reac}^{eq}
1 (eq 40)	39971	2.54×10^5	2
2 (eq 41)	37258	2.02×10^4	0.45

[a] Data taken from ref 32.

Table 3. Boiling Temperatures of Pure Components and Azeotropes at Atmospheric Pressure

component/mixture	composition (mol %)	boiling point (°C)
MeOH/DMC	87/13	63.8
MeOH		64.7
EtOH/EMC	95/5	74.9
EtOH/DMC	69/31	77.8
EtOH		78.4
DMC		90.4
EMC		107.9
DEC		126.5

chemical and pharmaceutical processes (e.g., production of polycarbonates and antibiotics).[29,30]

The reaction system consists of two consecutive reactions (eqs 40 and 41) with the intermediate product ethyl methyl carbonate (EMC). Both reactions are equilibrium limited, which prevents high DEC yields in conventional reactors.

$$\mathrm{DMC} + \mathrm{EtOH} \rightleftharpoons \mathrm{EMC} + \mathrm{MeOH} \tag{40}$$

$$\mathrm{EMC} + \mathrm{EtOH} \rightleftharpoons \mathrm{DEC} + \mathrm{MeOH} \tag{41}$$

Potassium carbonate (K_2CO_3) was suggested as an appropriate heterogeneous catalyst.[31] The reaction kinetics is described by a pseudo-homogeneous approach based on molar concentrations (eqs 42−45) and the required parameters are presented in Table 2.[32]

$$r_1 = k_{+1} x_{\mathrm{DMC}} x_{\mathrm{EtOH}} - k_{-1} x_{\mathrm{EMC}} x_{\mathrm{MeOH}} \tag{42}$$

$$r_2 = k_{+2} x_{\mathrm{EMC}} x_{\mathrm{EtOH}} - k_{-2} x_{\mathrm{DEC}} x_{\mathrm{MeOH}} \tag{43}$$

$$k_{+m} = k_{0,m} \exp\left(\frac{E_{A,m}}{RT}\right) \qquad (\text{for } m = 1, 2) \tag{44}$$

$$k_{-m} = \frac{k_{+m}}{K_{\mathrm{reac},m}^{\mathrm{eq}}} \qquad (\text{for } m = 1, 2) \tag{45}$$

The pure component and mixture properties of the components are described by means of the ASPEN Properties Database. The UNIQUAC model is chosen for the description of the thermodynamics of the mixture. Additional VLE data from the literature[33−38] are used to enhance the thermodynamics predictability of ASPEN Properties. The system does not have miscibility gaps; however, three binary homogeneous azeotropes exist. The boiling temperature of both the pure components and the azeotropes are presented in Table 3.

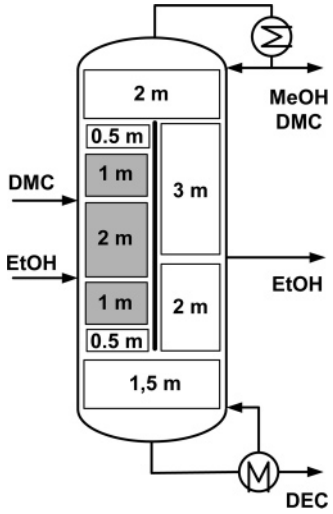

Figure 18. Reactive dividing wall column setup for DMC synthesis (gray area represents catalytic packing).

6.2. Column Setup. The transesterification of dialkyl carbonates by means of reactive distillation was first mentioned by Buysch et al.[39] Thereby, a homogeneous catalyst is applied, which complicates the later product purification. The usage of heterogeneous catalyst helps to avoid this difficulty, and the correspondent process has been studied recently by Richter et al.,[32] who showed that reactive distillation leads to significant increase in conversion and selectivity. However, the nonreacted reactants and products must be purified in an additional step, e.g., in a further nonreactive distillation column.

In this work, we consider the reactive distillation in the prefractionator equipped with a catalytic packing that contains a heterogeneous catalyst; this process is combined with a simultaneous separation of reactants and products in the main column, resulting in a reactive dividing wall column, as shown in Figure 18.

Sulzer BX packing with HETP ≈ 0.2 m is chosen for the nonreactive column section, whereas Multipak-II (HETP ≈ 0.24 m) is used as a catalytic packing. The column diameter is 0.28 m and the dividing wall is shifted to the side-draw side, resulting in a larger cross section of the prefractionator (the cross-sectional area ratio is 0.625).

The main column is equipped with 8.5 m of noncatalytic packing. The prefractionator contains 4.0 m of catalytic packing and 1.0 m of nonreactive packing. Because the reactants have different boiling temperatures (cf. Table 3), two separate feeds are used. The high-boiling reactant DMC is fed into the upper part of the reactive section, whereby the second feed, which contains the light-boiling EtOH, is allocated in the lower part. The use of the so-called "*double-feed configuration*" ensures an intensive contact of both reactants by counter-current flow between both feed locations. The proposed configuration was determined by varying different set-up parameters and it is still not optimized.

6.3. Operating Conditions. The molar ratio of EtOH to DMC in the feed streams is 3:1, which represents an excess of EtOH (the stoichiometric ratio is 2:1). Thereby, the reaction equilibrium is shifted more to the product side, which increases

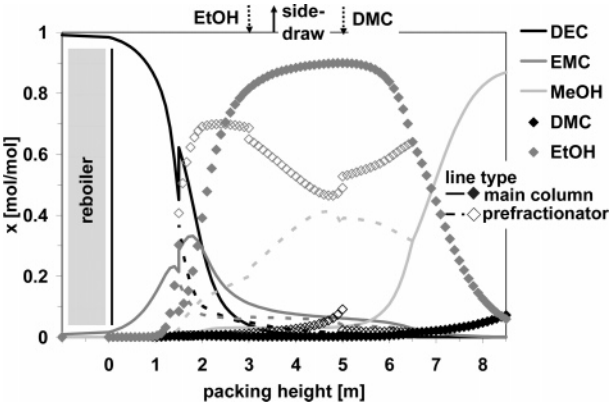

Figure 19. Simulated liquid-phase composition profiles.

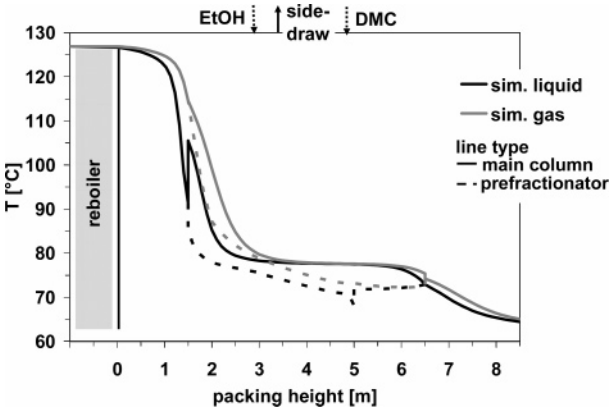

Figure 20. Simulated temperature profiles.

Table 4. Data Set

parameter	value
reflux ratio	11.67
$p_{\text{Condenser}}$	1.013 bar
$V_{\text{Feed DMC}}$	0.024 m^3/h
$T_{\text{Feed DMC}}$	75.0 °C
$V_{\text{Feed EtOH}}$	0.051 m^3/h
$T_{\text{Feed EtOH}}$	75.0 °C
$V_{\text{Top Product}}$	0.023 m^3/h
$V_{\text{Side Product}}$	0.027 m^3/h

conversion and selectivity within the column. Both feeds have a temperature of 75 °C, which is close to the boiling point of EtOH. Because reliable VLE data are only available at atmospheric pressure, the process is investigated for a condenser pressure of 1.013 bar. The reflux ratio is ∼11.67, which is quite high. However, one must remember that the reactive dividing wall column replaces at least two single columns. Thus, the total costs (including investment and operating costs) of the dividing wall column can be lower, even at such high reflux ratios. Furthermore, a later optimization of the column setup can probably lead to lower reflux ratios. All operating conditions are listed in Table 4.

6.4. Results. The simulations have been made without any adjusted parameters, and the heat transfer through the dividing wall has not been considered in this case. The nonreactive packing Sulzer BX is described using the correlations of Bravo et al.,[22,23] whereas for Multipak-II, the correlations of Hoffmann et al.[40,41] are used.

Figure 19 shows the simulated profiles for the liquid concentration in the reactive dividing wall column. In the prefractionator, EtOH accumulates in a high concentration (45−65 mol %), which is advantageous for the conversion and selectivity in the reactive zone. The high-boiling DMC is only present in low concentrations (<10 mol%). The byproduct MeOH is enriched toward the top of the prefractionator and leaves the column with the distillate stream, together with nonreacted DMC in a mixture close to the binary azeotrope of MeOH/DMC. The value product DEC can be obtained from the nearly pure bottom stream (∼99 mol %). The intermediate EMC and nonreacted EtOH are removed with the side-draw stream.

For the applied feedstock, the equilibrium conversion of DMC is ∼84%. This high value is due to the first reaction step, which lies on the intermediate side ($K^{\text{eq}}_{\text{reac}} = 2$). However, because the second reaction equilibrium is also on the intermediate side ($K^{\text{eq}}_{\text{reac}} = 0.45$), the selectivity of DMC to the main product DEC is low (42%). The simulation results of the reactive dividing wall column demonstrate that the combination of reaction and separation leads to a significant increase in selectivity (up to 73%). The conversion is kept almost constant at 87%.

The vapor flow rate split, which fits an equal pressure drop on both sides of the dividing wall, is 0.53, which is less than the cross-sectional area ratio of 0.625. This is caused by different packings, as the catalytic packing in the prefractionator has a higher vapor flow resistance than the noncatalytic packing in the main column. Initial studies show that the vapor flow rate ratio has a significant influence on the column performance (e.g., product purities) and, thus, cannot be simply set equal to the area ratio.

The temperature profiles for the liquid and vapor phase are shown in Figure 20. The temperature difference between the both sides of the dividing wall is <10 °C. Simulation studies of the heat transfer through the wall show that this phenomenon has no significant influence on the simulated purities and product yield. However, this effect generally should not be neglected, because it is dependent on many factors, e.g., column setup and hydrodynamics.

7. Conclusions

In this paper, a novel description of the nonreactive dividing wall column using the rate-based approach is suggested. Special attention is given to both the heat transfer through the dividing wall and the vapor flow rate split below the dividing wall, which have not been considered in previous works. The dividing wall column description has been extended to cover reactive systems, which results in a new configuration called the reactive dividing wall column. This process offers a higher degree of integration to achieve additional synergistic effects.

The model has been first applied to a nonreactive, ternary mixture of methanol, isopropanol, and butanol and further validated against the experimental data of Abdul Mutalib et al.[25] The comparison of simulated and measured concentrations and temperatures showed good agreement; however, significantly more experimental data are necessary to evaluate the model performance and the phenomenon of heat transfer through the dividing wall. The vapor flow rate ratio can be set equal to the cross-sectional area ratio, because the vapor resistances at both sides of the dividing wall are similar.

Furthermore, the transesterification of carbonates has been identified as an interesting system for the reactive dividing wall column. In first simulation studies, the conversion and selectivity could be significantly increased. At the same time, the dividing wall column offers a good separation of products and nonreacted reactants within the same apparatus. It was also shown that the vapor flow rate ratio differs from the area ratio, because of the

application of different types of packing (e.g., noncatalytic and catalytic packing), which significantly influences the column performance.

Nomenclature

a = specific interfacial area [m^2/m^3]
A = cross-sectional area [m^2]
ΔA^W = dividing wall area for a discrete (stage) [m^2]
c = concentration [mol/m^3]
D^{eff} = effective diffusivity [m^2/s]
$Đ$ = Maxwell−Stefan diffusion coefficient [m^2/s]
E_A = reaction activation energy [J/mol]
G = molar flow rate [mol/s]
H = specific enthalpy [J/mol]
(J) = vector of diffusional fluxes [mol/m^2s]
K^{eq} = vapor/liquid equilibrium constant
K^{eq}_{reac} = reaction equilibrium constant
k_0 = reaction frequency factor [$mol\ kg_{cat}^{-1}\ s^{-1}$]
$k_\pm$ = reaction velocity constant [$mol\ kg_{cat}^{-1}\ s^{-1}$]
k^W = heat-transfer coefficient for the dividing wall [$W\ m^{-2}\ K^{-1}$]
k^{eff} = effective mass-transfer coefficient [m/s]
$[k]$ = matrix of binary mass-transfer coefficients [m/s]
L = molar flow rate [mol/s]
N = interfacial molar flow rate [mol/m^2s]
n = number of components
p = pressure [Pa]
Q = heat flow rate [J/s]
q = heat flux [J/m^2s]
[R] = matrix defined by eqs 8−11 [s/m]
R = gas constant [$J\ mol^{-1}\ K^{-1}$]
r = reaction rate related to catalyst mass [$mol\ kg_{cat}^{-1}\ s^{-1}$]
s^W = thickness of the dividing wall [m]
T = temperature [K]
x = liquid-phase mole fraction [mol/mol]
V = volume flow [m^3/h]
y = vapor-phase mole fraction [mol/mol]
Δz = discrete (stage) height [m]

Greek Letters

α = heat-transfer coefficient of wall films [$W\ m^{-2}\ K^{-1}$]
$[\Gamma]$ = matrix of thermodynamic correction factors
δ = film thickness [m]
κ = binary mass-transfer coefficients [m/s]
λ = heat-conduction coefficient [$W\ m^{-1}\ K^{-1}$]
ρ_{cat} = catalyst density [kg/m^3]
Ψ_{cat} = catalyst volume fraction [m^3/m^3]
ϕ_{area} = cross-sectional area ratio (PF/total column) [m^2/m^2]
φ = flow rate ratios (PF/total column) [m^3/m^3]

Subscripts

G = gas phase
i, k = component index
j = stage index
L = liquid phase
m = reaction index
t = total

Superscripts

av = average
aDW = total stream above the dividing wall
aPF = stream at the upper dividing wall ending in prefractionator
aMC = stream at the upper dividing wall ending in main column
bDW = total stream below the dividing wall
bPF = stream at the lower dividing wall ending in prefractionator
bMC = stream at the lower dividing wall ending in main column
G = gas phase
I = interface
L = liquid phase
MC = main column
PF = prefractionator
W = dividing wall

Abbreviations

ACM = ASPEN Custom Modeler
DEC = diethyl carbonate
DMC = dimethyl carbonate
EMC = ethyl methyl carbonate
HETP = height equivalent to theoretical plate
i-PrOH = isopropanol
MeOH = methanol
NTSM = number of theoretical stages per meter
UNIQUAC = Universal-Quasi-Chemical (thermodynamic model)
VLE = vapor−liquid equilibrium

Acknowledgment

The support of the European Commission in the context of the 6th Framework Programme (INSERT, Contract No. NMP2-CT-2003-505862) is greatly acknowledged.

Literature Cited

(1) Noeres, C.; Kenig, E. Y.; Górak, A. Modelling of reactive separation processes: Reactive absorption and reactive distillation. *Chem. Eng. Process.* **2003**, *42*, 157−178.

(2) Petlyuk, F. B.; Platonov, V. M.; Slavinskii, D. M. Thermodynamically optimal method for separating multicomponent mixtures. *Int. Chem. Eng.* **1965**, *5*, 555−561.

(3) Shah, P. B. Squeeze more out of complex columns. *Chem. Eng. Prog.* **2002**, *97*, 46−55.

(4) Kaibel, G. Distillation columns with vertical partitions. *Chem. Eng. Technol.* **1987**, *10*, 92−98.

(5) Schultz, M. A.; Stewart, D. G.; Harris, J. M.; Rosenblum, S. P.; Shakur, M. S.; O'Brien, D. E. Reduce costs with dividing-wall columns. *Chem. Eng. Prog.* **2002**, *95*, 64−71.

(6) Adrian, T.; Schoenmakers, H.; Boll, M. Model predictive control of integrated unit operations: Control of a divided wall column. *Chem. Eng. Process.* **2004**, *43*, 347−355.

(7) Mueller, I.; Kloeker, M.; Kenig, E. Y. Rate-based modelling of dividing wall columns—a new application to reactive systems. In *PRES 2004, 7th Conference on Process Integration, Modelling and Optimisation for Energy Saving and Pollution Reduction*, Volume 4; Process Engineering Publisher: Prague, Czech Republic, 2004; pp 1325−1326.

(8) Mueller, I.; Kenig, E. Y. Integration of reaction and separation in a dividing wall column. In *Camure-5 & ISMR-4, 5th International Symposium on Catalysis in Multiphase Reactors & 4th International Symposium on Multifunctional Reactors*; Levec, J.; Pintar, A.; Eds.; National Institute of Chemistry: Ljubljana, 2005; pp 155−156.

(9) Kaibel, G. Method of carrying out chemical reactions and for the simultaneous fractionation of a mixture into several fractions by a distillation column. European Patent EP126,288 A2, 1984.

(10) Hill, T.; Kaibel, G.; Meyer, G.; Niekerken, J.; Schoenmakers, H. Reactive distillation apparatus for production of ethers from hydrocarbon fractions comprises simultaneous hydrogenation, etherification and distillative separation. German Patent DE10,033,958 A1, 2002.

(11) Becker, H.; Godorr, S.; Kreis, H. Partitioned distilliation columns—why, when & how. *Chem. Eng.* **2001**, (January), 68−74.

(12) Taylor, R.; Krishna, R.; Kooijman, H. Real-world modelling of distillation. *Chem. Eng. Prog.* **2003**, *7*, 28−39.

(13) Kenig, E. Y.; Górak, A. A film model-based approach for simulation of multicomponent reactive separation. *Chem. Eng. Process.* **1995**, *34*, 97−103.

(14) Kenig, E. Y.; Pyhälachti, A.; Jakobsson, K.; Górak, A.; Aittamaa, J.; Sundmacher, K. Advanced rate-based simulation tool for reactive distillation. *AIChE J.* **2004**, *50*, 332−342.

(15) Lewis, W. K.; Whitman, W. G. Principles of gas absorption. *Ind. Eng. Chem.* **1924**, *16*, 1215−1220.

(16) Górak, A.; Hoffmann, A. Catalytic distillation in structured packings: Methyl acetate synthesis. *AlChE J.* **2001**, *47*, 1067−1076.

(17) Kloeker, M.; Kenig, E. Y.; Schmitt, M.; Althaus, K.; Schoenmakers, H.; Markusse, P.; Kwant, G. Influence of operating conditions and column configuration on the performance of reactive distillation columns with liquid-liquid separators. *Can. J. Chem. Eng.* **2003**, *81*, 725−732.

(18) Krishna, R.; Standart, G. L. Mass and energy transfer in multicomponent systems. *Chem. Eng. Commun.* **1979**, *3*, 201−275.

(19) Toor, H. L. Solution of the linearized equations of multicomponent mass transfer. *AIChE J.* **1964**, *10*, 460−465.

(20) Stewart, W. E.; Prober, R. Matrix calculation of multicomponent mass transfer in isothermal systems. *Ind. Eng. Chem. Fundam.* **1964**, *4*, 224−235.

(21) Reid, R. C.; Prausnitz, J. M.; Poling, B. E. *The Properties of Gases and Liquids*, 4th Edition; McGraw−Hill: New York; 1987.

(22) Bravo, J. R.; Rocha, J. A.; Fair, J. R. Mass transfer in gauze packings. *Hydrocarbon Process.* **1985**, *64* (1), 91−95.

(23) Bravo, J. R.; Rocha, J. A.; Fair, J. R. Pressure drop in structured packings. *Hydrocarbon Process.* **1986**, *65* (3), 45−49.

(24) Lestak, F.; Smith, R.; Dhole, V. R. Heat transfer across the wall of dividing wall columns. *Trans. Inst. Chem. Eng.* **1994**, *72A*, 639−644.

(25) Abdul Mutalib, M. I.; Zeglam, A. O.; Smith, R. Operation and control of dividing wall distillation columns—Part 2: Simulation and pilot plant studies using temperature control. *Trans. Inst. Chem. Eng.* **1998**, *76A*, 319−334.

(26) Rocha, J. A.; Bravo, J. L.; Fair, J. R. Distillation columns containing structured packings: A comprehensive model for their performance. 1. Hydraulic models. *Ind. Eng. Chem. Res.* **1993**, *32*, 641−651.

(27) Rocha, J. A.; Bravo, J. L.; Fair, J. R. Distillation columns containing structured packings: A comprehensive model for their performance. 2. Mass-transfer model. *Ind. Eng. Chem. Res.* **1996**, *35*, 1660−1667.

(28) Abdul Mutalib, M. I. Operation and control of the dividing wall column, Ph.D. Dissertation, University of Manchester, Manchester, U.K., 1995.

(29) Parrish, J. P.; Salvatore, R. N.; Jung, K. W. Perspectives on alkyl carbonates in organic synthesis. *Tetrahedron* **2000**, *56*, 8207−8237.

(30) Luo, H.-P.; Xiao, W.-D. A reactive distillation process for a cascade and azeotropic reaction system: Carbonylation of ethanol with dimethyl carbonate. *Chem. Eng. Sci.* **2001**, *56*, 403−410.

(31) Angeletti, E.; Tundo, P.; Venturello, P. Gas-liquid phase-transfer catalysis: Catalytic and continous transesterification reaction. *J. Org. Chem.* **1983**, *48*, 4106−4108.

(32) Richter, J.; Zielinska-Nadolska, I.; Górak, A. Transesterification of dimetyl carbonate via reactive distillation. In *PRES 2004, 7th Conference on Process Integration, Modelling and Optimisation for Energy Saving and Pollution Reduction*, Volume 4; Process Engineering Publisher: Prague, Czech Republic, 2004; pp 1328−1329.

(33) Comelli, F.; Francesconi, R.; Ottani, S. Isothermal vapor−liquid equilibria of dimethyl carbonate + diethyl carbonate in the range (313.15 to 353.15) K. *J. Chem. Eng. Data* **1996**, *41*, 534−536.

(34) Luo, H.; Xiao, W.; Zhu, K. Isobaric vapour−liquid equilibria of alkyl carbonates with alcohols. *Fluid Phase Equilib.* **2000**, *175*, 91−105.

(35) Luo, H.; Zhou, J.; Xiao, W.; Zhu, K. Isobaric vapor−liquid equilibria of binary mixtures containing dimethyl carbonate under atmospheric pressure. *J. Chem. Eng. Data* **2001**, *46*, 842−845.

(36) Rodríguez, A.; Canosa, J.; Domínguez, A.; Tojo, J. Isobaric phase equilibria of diethyl carbonate with five alcohols at 101.3 kPa. *J. Chem. Eng. Data* **2003**, *48*, 86−91.

(37) Gmehling, J.; Menke, J.; Fischer, K.; Krafczyk, J. *Azeotropic Data, Part I*; Wiley−VCH: Weinheim, Germany, 1994.

(38) Rodríguez, A.; Canosa, A. J. Domínguez; Tojo, J. Vapour-liquid equilibria of dimethyl carbonate with linear alcohols and estimation of interaction parameters for the UNIFAC and ASOG method. *Fluid Phase Equilib.* **2002**, *201*, 187−201.

(39) Buysh, H.-J.; Klausener, A.; Langer, R.; Mais, F.-J. Process for the continuous preparation of dialkyle carbonates. German Patent DE4,129,316 A1, 1991.

(40) Hoffmann, A.; Noeres, C.; Górak, A. Scale-up of reactive distillation columns with catalytic packings. *Chem. Eng. Process.* **2004**, *43*, 383−395.

(41) Hoffmann, A. Scale-up von Rektifikationskolonnen mit katalytischen Packungen, Ph.D. Dissertation, University of Dortmund, Dortmund, Germany, 2005.

Received for review August 7, 2006
Revised manuscript received February 23, 2007
Accepted March 5, 2007

IE0610344